Journal of Power Sources 196 (2011) 7442–7449

Contents lists available at ScienceDirect

Journal of Power Sources

journal homepage: www.elsevier.com/locate/jpowsour

A corrugated mesoscale structure on electrode–electrolyte interface for enhancing cell performance in anode-supported SOFC

Akio Konno*, Hiroshi Iwai, Motohiro Saito, Hideo Yoshida

Department of Aeronautics and Astronautics, Kyoto University, Yoshida Honmachi, Sakyo-ku, Kyoto 606-8501, Japan

ARTICLE INFO

Article history:
Received 18 January 2011
Received in revised form 6 April 2011
Accepted 21 April 2011
Available online 30 April 2011

Keywords:
Anode-supported SOFC
Mesoscale structure
Corrugated electrolyte
Interface area enlargement
Numerical simulation

ABSTRACT

For enhancing the power density of a solid oxide fuel cell, mesoscale-structure control of electrode–electrolyte interfaces in an anode-supported cell is proposed. We define 'mesoscale' as a size range of the order of 10–100 μm which is larger than the 'microscale' of electrode particles but smaller than the 'macroscale' of cell geometries. Mesoscale-structure control enlarges the electrode–electrolyte interface, and this enlargement extends an active electrochemical reaction zone where a charge-transfer reaction occurs actively near the interface. A corrugated mesoscale electrolyte was adopted which enlarged the interface structures of both anode and cathode sides. We performed a 2-D numerical simulation, and discussed the effects of such structure not only on the overall performance but also on the detailed distributions of electric potentials, gas concentrations and local electrochemical reaction rate. As a result, it was observed that the corrugated mesoscale structure reduced both activation overpotential and ohmic loss by ion transport, and hence enhanced the power generation performance. When the interface area enlargement factor was 1.73, an enhancement of a power density having a maximum value of 59% was achieved with the mesoscale-corrugated cell rather than with the flat cell.

1. Introduction

Solid oxide fuel cells (SOFCs) directly convert the chemical energy of gases into electrical energy. Owing to their high efficiencies, SOFCs are regarded as future power generation systems. However, the durability and cost of the SOFC system are principal issues that need to be addressed prior to the commercialization of SOFCs. In addition, reducing the start-up time is important for many applications. Increasing the power density of the system is another fundamental and important study because it reduces the size, weight and the material cost of the system, and enhances the load-following capability attributed the decrease in the heat capacity.

Various methods for increasing the power density of SOFCs have been proposed and investigated. Material development is one major method for improving the power density. In this study we focus on methods based on geometric control which can be classified into three categories depending on the characteristic length of the geometry. The first category is macroscopic control of cell design [1–5] which generally has a characteristic length of the order of greater than 1 mm. For example, a stack composed of planar cells generally has a cell surface area larger than that of a stack of tubular cells of the same size. The surface area density of tubular cells can be improved by reducing the tube diameter (micro-tubular SOFC) [4]. According to the authors' understanding, mono-block-layer built (MOLB)-type cells [5] also belong to this category.

The second category is microstructure control which generally has a characteristic length of the order of less than 1 μm. This is attributed to various parameters of the porous electrode microstructure such as volume fraction, the tortuosity factor and the three-phase boundary (TPB). By tuning calcination and sintering conditions (temperature and time) or by changing the primary-particle diameter, the microstructure of the porous electrodes can be statistically controlled [6–9]. Because the microstructure directly affects the active electrochemical reaction site, this approach can be effective for enhancing the cell performance as long as the problem of degradation problem due to the morphology change in a long-term operation [9–11] is solved.

The third category is mesoscale-structure control which we have proposed in a recent article [12], the characteristic length of which is of the order 10–100 μm. We have reported the effects of the anode–electrolyte interface shape control on cell performance in this scale range [12]. As one of the simplest mesoscale structures, we applied a wavy shape on the anode–electrolyte interface which increased the active electrochemical reaction zone spreading in the vicinity of the interface. The interface enlargement was determined to be effective when the characteristic length of the wavy interface was larger than the effective thickness of the electrode. Although similar surface enlargement concepts seem to be observed in the macroscale (MOLB-type cell) and in the microscale

* Corresponding author. Tel.: +81 75 753 5203; fax: +81 75 753 5203.
E-mail address: konno@t06.mbox.media.kyoto-u.ac.jp (A. Konno).

0378-7753/$ – see front matter © 2011 Elsevier B.V. All rights reserved.
doi:10.1016/j.jpowsour.2011.04.051

Nomenclature

d	diameter (m)
E_0	EMF at standard state (V)
F	Faraday constant (C mol^{-1})
I	current (A)
i	current density (A m^{-2})
$i_0{}^L$	exchange current per unit TPB length (A m^{-1})
i_{ct}	volume-specific charge transfer current (A m^{-3})
l	thickness or height (m)
l_{tpb}	TPB density (m^{-2})
P	pressure or partial pressure (Pa)
p	percolation probability
R_0	universal gas constant (J mol^{-1} K^{-1})
T	temperature (K)
V	volume of computational domain
v	volume fraction
w	width (m)
X	molar fraction

Greek symbols

α_{area}	interface area enlargement factor
ε	porosity
η	overpotential (V)
η_{cell}	total cell overpotential (V)
τ	tortuosity factor
ϕ	potential (V)
ϕ_0	Nernst potential (V)
ϕ_{FC}	cell terminal voltage (V)

Subscripts

act	activation
amp	amplitude
ano	anode
ave	average value
bulk	bulk fluid
cath	cathode
ct	charge transfer
con	concentration
el	electron-conducting phase
ele	electrolyte
int	electrode–electrolyte interface
io	ion-conducting phase
ohm	ohmic
per	period
t	total
tpb	three-phase boundary

Superscripts

L	per unit length
m	mean value

(surface roughness control), the characteristic length in our study is smaller than in the macroscale and larger than that in the microscale. It should be noted that, in principle, we can simultaneously apply or superimpose these surface enlargement concepts with the different characteristic lengths. Hence, the approach with the present geometric characteristic length is of significant importance.

In our previous report on mesoscale control, we employed electrolyte-supported cells as test cells. However, through a discussion on the relative comparison between reaction resistivity and ion transport resistivity of the electrolyte, it was suggested that surface enlargement by a wavy interface is most effective

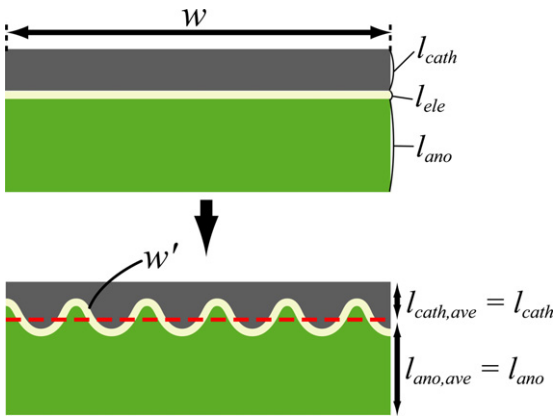

Fig. 1. Schematic diagram of corrugated mesoscale-structure control in electrode-supported cell.

when the electrolyte is thin [12]. Because a suitable mesoscale structure design as well as its optimization is desired, in this study, we numerically investigate the effect of electrolyte corrugation on the performance of anode-supported cells using a thin electrolyte layer. The effectiveness of this mesoscale-structure control is discussed on the basis of the distributions of electric potential, gas concentration, overpotential and charge transfer current.

2. Computational conditions and procedure

2.1. Computational domain and simulation method

Fig. 1 schematically shows a situation in which the corrugated electrolyte increases the electrode–electrolyte interface area with respect to an apparent electrode area of an anode-supported cell. Here the apparent electrode area denotes the projected area perpendicular to the direction of cell thickness. In this study we address with the case of a rectangular corrugation, for simplicity. By applying the rectangular shape instead of sinusoidal wavy shape, we can clearly separate the electrode into two regions having distinct thicknesses. It is suitable for discussion of gas diffusion. Fig. 2 shows the computational domain. A symmetric boundary condition is applied in the x-direction for reducing the computational time. We assume a cell composed of conventional materials, containing a nickel–yttria stabilized zirconia (Ni–YSZ) cermet anode, a thin YSZ electrolyte and a thin lanthanum strontium manganate (LSM)–YSZ cathode. Because the simulation procedure is the same as that described in the previous study [12], it is only briefly explained here. We performed a steady two-dimensional simulation assuming a constant and uniform temperature of 800 °C. The microstructure of the porous electrodes was modeled by the random packing of spheres [13,14] with a constant and uniform particle diameter for both ionic and electronic conductors in the electrodes. We considered oxide ion, electron and mass transports in the electrodes, whereas in the electrolyte, we considered only ion transport. The dusty-gas model [15,16] was used for mass transport in the porous electrodes. This model considers the flow induced by a total pressure gradient and can also be used for the situation in which the effect of Knudsen diffusion is not negligible. The evaluation of the charge transfer current on the TPB is presented in a later section. Combining these models, we calculated the distributions of the electric potentials of electron- and ion-conducting phases, the gas concentration and the local electrochemical reaction rate (charge transfer current) [12,13].

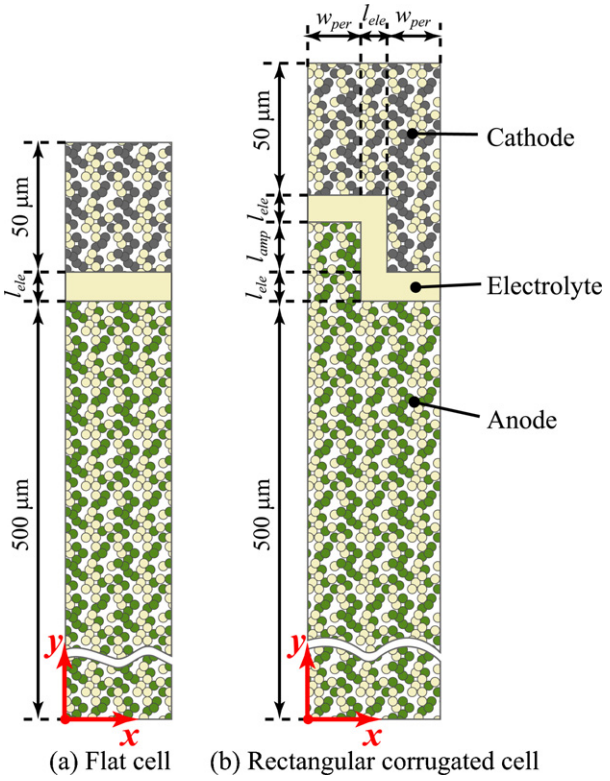

Fig. 2. Computational model of (a) flat cell and (b) rectangular corrugated cell.

2.2. Geometries of cells with electrolyte corrugation

The geometric parameters of the corrugated electrolyte examined in this study are summarized in Table 1; their shapes and the lengths, of w_{per} and l_{amp}, are schematically shown in Fig. 3. The interface area enlargement factor, α_{area}, is defined simply as follows:

$$\alpha_{area} = \frac{2w_{per} + l_{amp}}{2w_{per} + l_{ele}} \quad (1)$$

To capitalize on the enlargement of the interface, the characteristic length of the corrugation needs to be larger than the effective thickness of the electrode, approximately 10 µm [12]. Hence, the characteristic length of the corrugation was set at about 50–100 µm in this study. The shortest distances from the electrode surface to the electrode–electrolyte interface were fixed for all electrodes: 50 µm on the cathode side and 500 µm on the anode side (the total thickness of the cell varied with the corrugation amplitude l_{amp}). As a result, it should be noted that a cell with a standard flat interface without corrugation is always in a better condition than the corrugated cells from the view point of concentration overpotential.

Table 1
Mesoscale parameters of rectangular corrugated cell.

	w_{per} (µm)	l_{amp} (µm)	l_{ele} (µm)	α_{area}
Case 1	100	40	10	1.14
Case 2	75	40	10	1.19
Case 3	50	40	10	1.27
Case 4	100	90	10	1.38
Case 5	75	90	10	1.50
Case 6	50	90	10	1.73

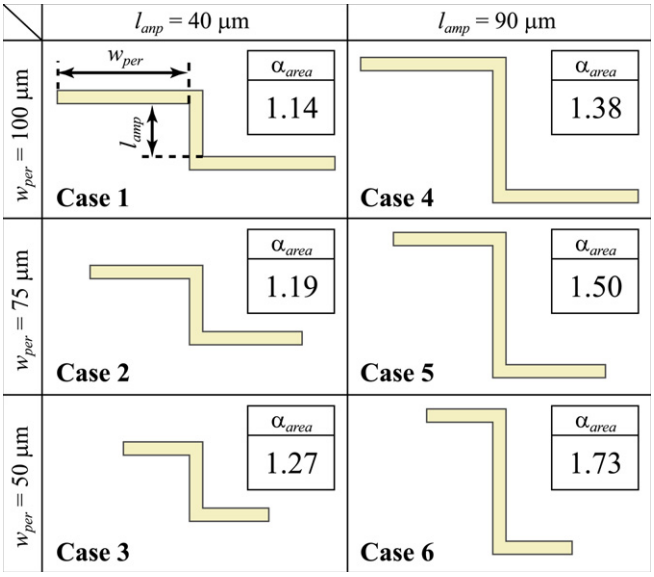

Fig. 3. Six cases with different mesoscale-corrugated electrolytes.

2.3. Electrochemical reaction model

In the electrochemical reaction model, the volume-specific charge transfer current on the TPB was calculated from the reaction equation given by Eq. (2):

$$i_{ct} = i_0^L l_{tpb} \left[\exp\left(\frac{F}{R_0 T}\eta_{act}\right) - \exp\left(\frac{-F}{R_0 T}\eta_{act}\right) \right] \quad (2)$$

where l_{tpb} is the volume-specific length of the TPB in porous electrodes evaluated by the random packing model of spheres, while $i_0{}^L$ is the exchange current per unit TPB length evaluated by the following empirical equations for the anode [17,18] and the cathode [19], respectively:

$$i_{0,ano}^L = 31.4 P_{H_2}^{-0.03} P_{H_2O}^{0.4} \exp\left(\frac{-18,300}{T}\right) \quad (3)$$

$$i_{0,cath}^L = 1.10 P_{O_2}^{0.5} \exp\left(\frac{-16,500}{T}\right) \quad (4)$$

2.4. Calculation and boundary conditions

Table 2 summarizes the calculation conditions. The total pressure and gas composition at the electrode surface were maintained constant. The properties of the porous electrodes were evaluated by the random packing model [13,14] by assuming uniform particle diameters for the electron- and ion-conducting phases, d_{el} and d_{io}, respectively. The percolation probability and TPB density in Table 2 were evaluated on the basis of these assumptions. Fig. 4 shows the boundary conditions. We applied a symmetric boundary condition in the horizontal (x) direction. The electric potential of the electron-conducting phase at the anode surface was set at the Nernst potential calculated using with Eq. (5), while the cell terminal voltage, ϕ_{FC}, applied at the cathode surface was varied in order to change the power generation condition.

$$\phi_0 = E_0 + \frac{RT}{2F} \ln\left(\frac{P_{H_2,bulk}}{P_{H_2O,bulk}}\left(\frac{P_{O_2,bulk}}{10,130}\right)^{0.5}\right) \quad (5)$$

2.5. Evaluation of losses

The ohmic, activation and concentration losses measured in the experiments were regarded as macroscopic values based on the

Table 2
Calculation conditions.

Calculation parameter	Anode	Cathode
Operating temperature T (°C)	800	800
Total pressure P_t (MPa)	0.1013	0.1013
Gas compositions	$X_{H_2} : X_{H_2O} = 0.99 : 0.01$	$X_{O_2} : X_{N_2} = 0.21 : 0.79$
Tortuosity factor τ	3.0	3.0
Porosity ε	0.3	0.3
Volume fraction of electron-conducting phase v_{el}	0.35	0.35
Volume fraction of ion-conducting phase v_{io}	0.35	0.35
Particle diameter of electron-conducting phase d_{el} (μm)	1	1
Particle diameter of ion-conducting phase d_{io}(μm)	1	1
Percolation prob. of electron-conducting phase p_{el}	0.925	0.925
Percolation prob. of ion-conducting phase p_{io}	0.925	0.925
TPB density l_{tpb} (μm^{-2})	1.40	1.40

local distributions. Therefore, for such a conventional discussion of cell performance, it is useful to evaluate the representing mean values for each loss on the basis of the simulation results, as follows.

2.5.1. Activation and concentration losses

We can write the mean values as Eqs. (6) and (7).

$$\eta^m_{\mathrm{act,ano}} = \frac{\int \eta_{\mathrm{act,ano}} i_{\mathrm{ct}} dV}{I_t}, \qquad \eta^m_{\mathrm{act,cath}} = \frac{\int \eta_{\mathrm{act,cath}} i_{\mathrm{ct}} dV}{I_t} \tag{6}$$

$$\eta^m_{\mathrm{con,ano}} = \frac{\int \eta_{\mathrm{con,ano}} i_{\mathrm{ct}} dV}{I_t}, \qquad \eta^m_{\mathrm{con,cath}} = \frac{\int \eta_{\mathrm{con,cath}} i_{\mathrm{ct}} dV}{I_t} \tag{7}$$

where I_t and i_{ct} are the total current and the local charge transfer current, respectively, and V is the volume of the computational domain.

2.5.2. Ohmic loss

We define the local ohmic loss as the potential difference between an arbitrary point in the electrode and a reference potential. It can be calculated if a definite reference potential can be specified at the reference point. Because the electric potential of the electron-conducting phase at the electrode surface was uniform and constant in this study, we set the reference point at the electrode surface for the electron transport. We calculated the representing mean ohmic loss associated with electron transport as:

$$\eta^m_{\mathrm{ohm,el,ano}} = \frac{\int (\phi_0 - \phi_{\mathrm{el}}) i_{\mathrm{ct}} dV}{I_t},$$

$$\eta^m_{\mathrm{ohm,el,cath}} = \frac{\int (\phi_{\mathrm{el}} - \phi_{\mathrm{FC}}) i_{\mathrm{ct}} dV}{I_t} \tag{8}$$

For the case of ion transport, it is possible to set the reference point at the electrode–electrolyte interface if the cell is flat. In this case, we can write the mean ohmic loss associated with ion transport in the electrode as:

$$\eta^m_{\mathrm{ohm,io,ano}} = \frac{\int (\phi_0 - \phi_{\mathrm{int,ano}}) i_{\mathrm{ct}} dV}{I_t},$$

$$\eta^m_{\mathrm{ohm,io,cath}} = \frac{\int (\phi_{\mathrm{int,cath}} - \phi_{\mathrm{io}}) i_{\mathrm{ct}} dV}{I_t} \tag{9}$$

However, when the interface has a mesoscale structure, a definite reference potential cannot be specified anywhere in the electrodes. Hence, for the case of corrugated cells, we calculated the representing mean ohmic loss associated with ion transport as the difference between the total loss of the cell and the sum of the losses expressed by Eqs. (6)–(8):

$$\eta^m_{\mathrm{ohm,io}} = \eta_{\mathrm{cell}} - \sum_i \eta^m_i = \phi_0 - \phi_{\mathrm{FC}} - \eta^m_{\mathrm{con,ano}} - \eta_{\mathrm{ohm,el}},$$

$$\mathrm{ano}^m - \eta^m_{\mathrm{act,cath}} - \eta^m_{\mathrm{con,cath}} - \eta^m_{\mathrm{ohm,el,cath}} \tag{10}$$

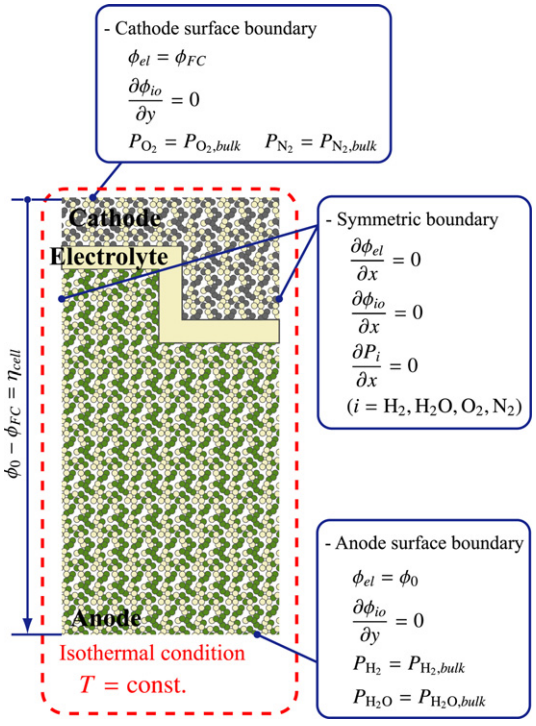

Fig. 4. Calculation and boundary conditions.

3. Results and discussion

3.1. Effect of corrugated structure on distributions of reaction field

First, we discuss the fundamental influences of the corrugated structure on distributions, such as the gas partial pressure, the electric potentials of electron- and ion-conducting phases, the activation overpotential, the concentration overpotential and the volume-specific charge transfer current. We focus our discussion on the results of Case 4, with an average current density of 1000 mA cm^{-2}; average current density is defined as the value of the total current divided by the apparent electrode area.

Fig. 5 shows partial and total pressure distributions: (a) partial pressure of oxygen for the cathode and of hydrogen for the anode, (b) partial pressure of nitrogen for the cathode and of water vapour for the anode, and (c) total pressure fields in the cathode and anode. Note that the value of the colour contour differs in each

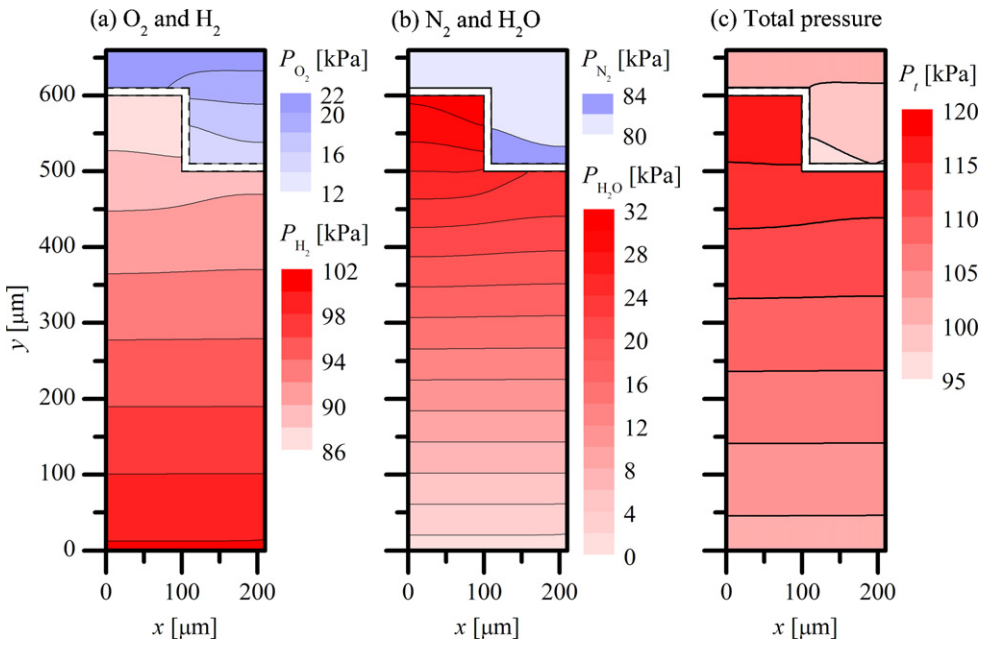

Fig. 5. Pressure distributions of (a) O_2–H_2 partial pressure, (b) N_2–H_2O partial pressure and (c) total pressure, for Case 4.

distribution. Because oxygen and hydrogen diffusing from the electrode surfaces were consumed in the vicinity of the cathode– and anode–electrolyte interfaces, respectively, these partial pressures decreased with increasing electrode depths. On the other hand, the partial pressure of water vapour produced on the anode-side increased with the electrode depth. In addition, the partial pressure of nitrogen on the cathode-side increased with the electrode depth because nitrogen was driven to the interface by a total pressure gradient caused by oxygen consumption in the vicinity of the interface. In addition to the above-mentioned features, primarily in the vertical direction of the figures, we can distinctly observe the effects of the corrugated structure on the pressure difference along the electrode–electrolyte interface.

Fig. 6a and b shows the electric potential distributions of electron- and ion-conducting phases, respectively. The electric potential of the electron-conducting phase shown in Fig. 6a is almost uniform in both electrodes because of high electronic conductivities; this implies that the effect of electronic conduction on the cell performance in the electrodes was negligible. On the other hand, the electric potential of the ion-conducting phase shown in Fig. 6b significantly changed around the electrolyte because the charge transfer reaction occurred in the vicinity of the electrode–electrolyte interface. The ohmic loss was caused by the ionic current that flowed through the electrolyte from the cathode to the anode.

Fig. 7a shows the distribution of the activation overpotential evaluated from the electric potentials and the concentration overpotential. It can be determined from this figure that the trend of the activation overpotential almost corresponds to that of the electric potential of the ion-conducting phase. Fig. 7b shows the distribution of the concentration overpotential. Because concentration overpotential depends on partial pressure, it increases in the regions of diluted oxygen for the cathode and of diluted hydrogen and concentrated water vapour for the anode. The concentration overpotential was negligibly small on the cathode side and had a maximum value of approximately 0.16 V on the anode side. The variation of the concentration overpotential along the anode–electrolyte interface was found to be less than 0.02 V. Hence, it was observed that the differences in the concentration overpotential in the reaction zone of each electrode were relatively small.

Fig. 8 shows the distribution of the volume-specific charge transfer current focused around the electrolyte. The charge transfer current takes high values in the region near the electrolyte. We define an active reaction zone as the zone where the volume-specific charge transfer current is more than 10% of its maximum value. In this figure, the dashed-red lines show the outer limit of the active reaction zones on both anode and cathode sides. (For interpretation of the references to colour in this figure text, the reader is referred to the web version of this article.) It can be observed from Fig. 8 that the thickness of the active reaction zone is approximately 20 μm on anode side and 10 μm on cathode side. This figure indicates that the trend of the charge transfer current agrees with those of the activation overpotential and electric

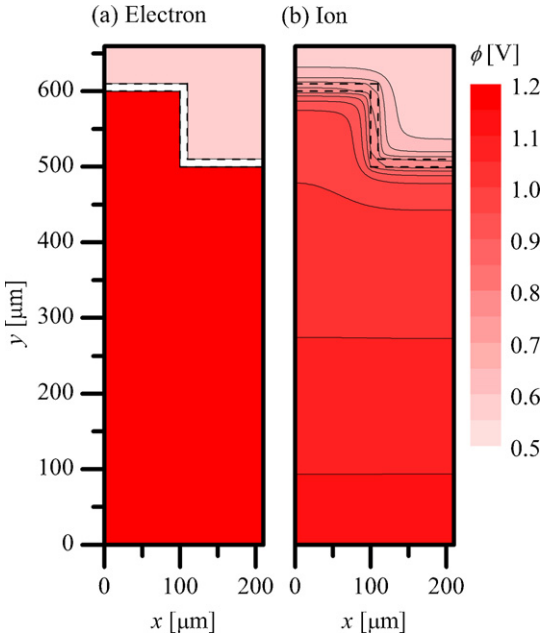

Fig. 6. Electric potential distributions of (a) electron- and (b) ion-conducting phases for Case 4.

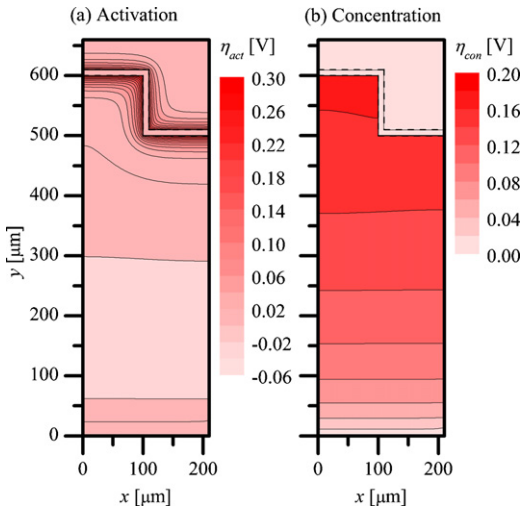

Fig. 7. Overpotential distributions of (a) activation and (b) concentration, for Case 4.

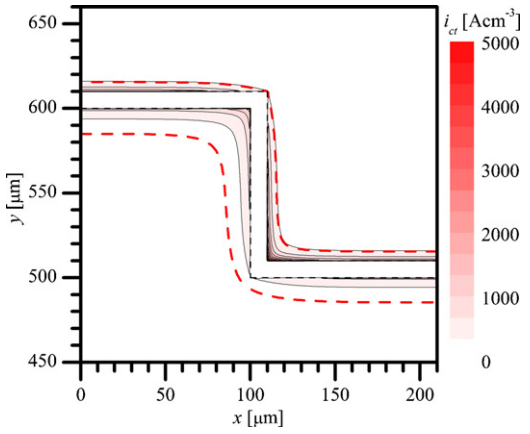

Fig. 8. Volume-specific charge transfer current distribution with active reaction zone around electrolyte for Case 4.

potential of the ion-conducting phase. From this result, the active reaction zone was found to strongly depend on the electric potential of the ion-conducting phase. For comparison, the distribution of the volume-specific charge transfer current for Case 1 is illustrated in Fig. 9. The active reaction zone is also marked in this figure. The active reaction zones for Case 1 also distributes in the electrodes within 20 μm for anode and 10 μm for cathode from each electrode interfaces. In Case 1, the variation of the concentration overpotential along the anode–electrolyte interface was even smaller than Case 4 and was less than 0.01 V. Although slight difference is observed in the variation of the concentration overpotential along the interfaces between Cases 1 and 4, its effect on the active reaction zone is limited. There was no appreciable difference in the active reaction zones between Cases 1 and 4. Hence, the positive effect of increasing the amplitude of the corrugated structure was superior to the negative effect associated with increasing the concentration overpotential. As intended, this effective thickness of the reaction zone was determined to be much smaller than the scale of the corrugated structure. Thus, the enlargement of the reaction zone by the corrugated structure resulted in a reduction in the local charge transfer and ionic current, thereby reaching the overpotential reductions and consequently enhancing cell performance.

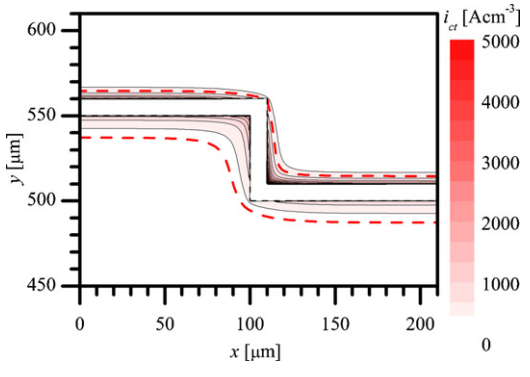

Fig. 9. Volume-specific charge transfer current distribution with active reaction zone around electrolyte for Case 1.

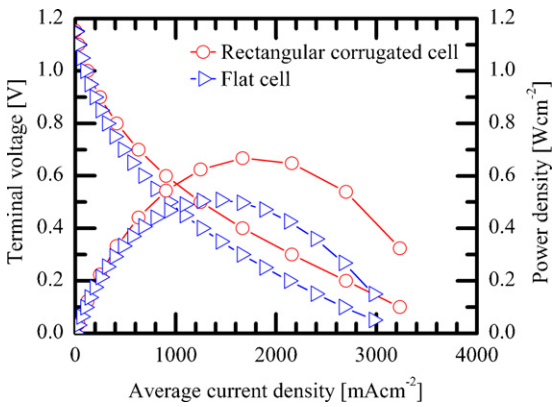

Fig. 10. Characteristics of *i*–*V* and *i*–*P* for Case 4.

3.2. Overall cell performance

Fig. 10 shows the *i*–*V* and *i*–*P* characteristics for Case 4 together with the results for a flat cell. It was observed that the mesoscale-corrugated cell enhanced the power generation performance compared to the flat cell. The maximum power density for Case 4 is 32% higher than that for the flat cell. This improvement was achieved because the positive effect, primarily caused by the interface enlargement, was more prominent than the negative effects associated with the increased concentration overpotential and the ohmic loss.

Fig. 11 shows the average current density enhancement, defined as the ratio of the average current density of a corrugated cell to that

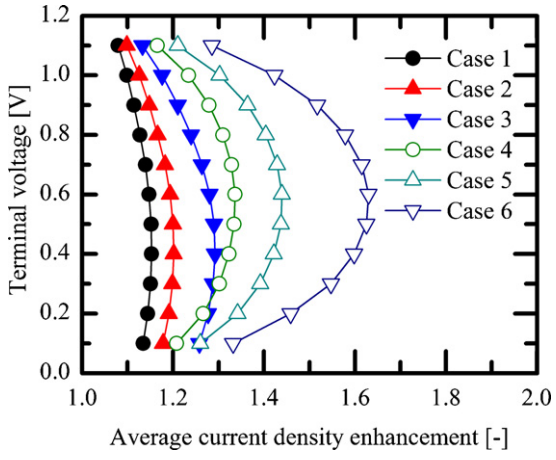

Fig. 11. Average current density enhancement by corrugated electrolyte.

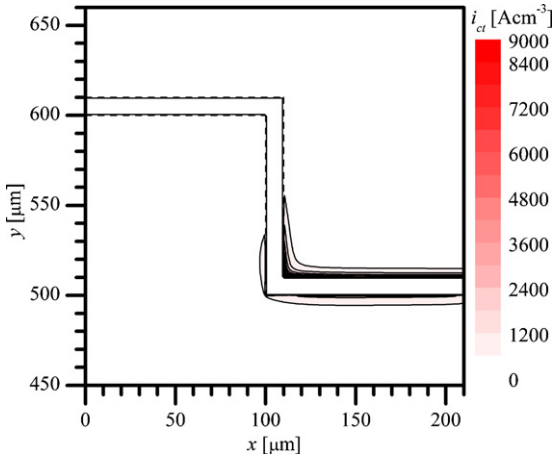

Fig. 12. Volume-specific charge transfer current distributions for Case 4 at average current density of 1000 mA cm^{-2} under low anode porosity condition (ε_{ano} = 0.1).

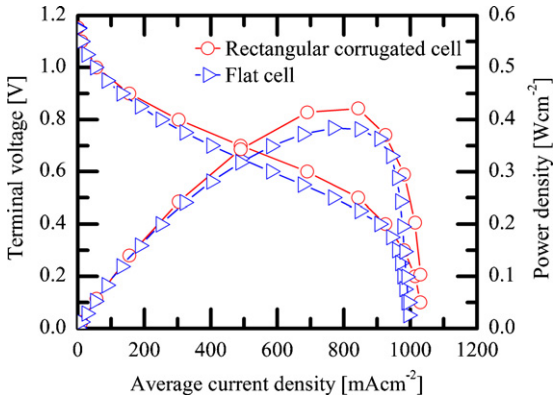

Fig. 13. Characteristics of i–V and i–P under low anode porosity condition (ε_{ano} = 0.1).

of a flat cell at the same terminal voltage, as follows:

$$\text{Average current density enhancement} = \frac{\text{Average current density of corrugated cell}}{\text{Average current density of flat cell}} \quad (11)$$

Solid symbols indicate cases with shallow corrugation (Cases 1–3), whereas solid-white symbols indicate cases with deep corrugation (Cases 4–6). The figure shows that, in all cases, the average current density enhancement takes a value larger than unity. The degree of enhancement is closely related to the interface area enlargement factor of the corrugated cell. A cell with a larger interface enlargement factor results in a larger average current density enhancement. Case 6 achieved an enhancement of 63% at a terminal voltage of 0.6 V. It is also noted that there exists a maximum value of the average current density enhancement for each case. That is, starting from the higher terminal voltage, the average current density enhancement increases as the terminal voltage decreases. The decrease at the relatively low terminal voltage range is ascribed to the increase of the concentration overpotential due to the relatively high current density, and its effect is more prominent in the cases with deep corrugation (Cases 4–6). The maximum value is obtained at relatively high terminal voltage for the deep-corrugation cases because the effect of the concentration overpotential increases with the increasing depth of the electrode. Hence, the effect of the concentration overpotential cannot be neglected for the deep-corrugation case and for the relatively high average current density condition.

Table 3 summarizes the mean losses of the cells calculated at an average current density of 1000 mA cm^{-2}. The three mean ohmic losses by ion transport in each component (cathode, anode and electrolyte) are shown separately in the flat cell, while the total value of the mean ohmic loss by ion transport is shown for the corrugated cells because the mean ohmic loss of the corrugated cell cannot be separated into cell components as explained in Section 2.5. The mean ohmic loss by electron transport and the mean cathode concentration overpotential were negligibly small compared to the total loss. The mean anode concentration overpotential was relatively large but was not affected by the corrugated shape under the conditions indicated in Table 3. The total ohmic loss by ion transport and the mean activation overpotential in the mesoscale-corrugated cells considerably decreased with increase in the interface area enlargement factor. This confirms the positive effect of the reduced local current by the interface area enlargement. Table 4 shows the maximum power density of the cells. The maximum power density is increased by the interface area enlargement factor and is enhanced by 59% for Case 6.

3.3. Effect of porosity

It was shown in the previous discussion with the help of Fig. 11 that the degree of performance enhancement can be suppressed by the concentration overpotential even though the porosity in the porous electrodes is assumed to be reasonably high in the above calculations. Hence we examine the effect of the anode porosity reduced from its original value of 0.3–0.1. We focus on the anode

Table 3
Total and mean overpotentials at average current density of 1000 mA cm^{-2}.

	Flat	Case 1	Case 2	Case 3	Case 4	Case 5	Case 6
Total (mV)	674	629	617	595	583	560	525
Reduction (%)		6.6	8.5	11.7	13.5	16.8	22.1
Cathode							
Ohm (electron) (mV)	0.02	0.03	0.03	0.03	0.05	0.05	0.05
Ohm (ion) (mV)	73						
Activation (mV)	118	111	109	105	101	96	89
Concentration (mV)	1.68	3.22	3.33	3.52	5.19	5.43	5.82
Anode							
Ohm (electron) (mV)	0.01	0.01	0.01	0.01	0.01	0.01	0.01
Ohm (ion) (mV)	121						
Activation (mV)	161	147	144	137	127	120	109
Concentration (mV)	153	154	154	155	157	158	158
Electrolyte							
Ohm (ion) (mV)	45						
Total							
Ohm (ion) (mV)	240	213	206	194	192	181	163

Table 4
Maximum power density and its enhancement for certain cases.

	Flat	Case 1	Case 2	Case 3	Case 4	Case 5	Case 6
Maximum power density ($mW\,cm^{-2}$)	507	581	606	652	667	717	806
Enhancement (%)		15	19	28	32	41	59

side not only because we assume an anode-supported cell in this study but also because its porosity may change during a long-term operation. The microstructure may change for various reasons such as thermal cycle, redox cycle and carbon deposition.

Fig. 12 shows the distribution of the volume-specific charge transfer current for a case with a low-porosity anode. Other conditions were the same as those shown in Fig. 8. The active reaction zone in which the charge transfer reaction proceeds was distributed unevenly in one side ($y \sim 500\,\mu m$) while the local charge transfer current was concentrated into this side. The vertical part was not effectively used either. The active side was closer to the anode surface and so the anode gas transport was relatively better than that of the other side ($y \sim 600\,\mu m$). This figure indicates that less than half of the electrode–electrolyte interface region was active in this case.

Fig. 13 shows the characteristics of i–V and i–P for this case, along with the results for a flat cell. The porosity of the anode was 0.1 for the flat case also. The i–V characteristics clearly indicate the maximum current density due to the concentration overpotential at the high current density. Greater performance enhancement of the corrugated cell than the flat cell was not observed under this condition. Hence, the corrugated mesoscale structure was not useful in this case. The effect of the concentration overpotential needs to be carefully examined for designing an effective corrugated shape.

4. Conclusion

A 2-D numerical simulation was performed to understand the effect of corrugated-mesoscale structure control in an anode-supported cell containing a thin electrolyte on power generation performance. A flat-cell case in addition to six cases of the corrugated mesoscale structure with different interface area enlargement factors were calculated. We reported the following results.

(1) The mesoscale-corrugated cell enhanced the power generation performance compared to the flat cell because the local ionic current around the electrolyte was reduced due to interface enlargement. From the viewpoint of the representing mean voltage losses, the mean ohmic loss by ion transport and the mean activation overpotential of both electrodes decreased with increasing interface area enlargement. This was a result of the reduced local ionic current.
(2) The active reaction zone was distributed in the electrodes up to 20 μm from the electrode–electrolyte interface under the conditions in this study, and it strongly depends on the electric potential distribution of the ion-conducting phase.
(3) The degree of enhancement was closely related to the interface area enlargement factor of the corrugated cell. There existed a maximum value of the average current density enhancement for each case because the effect of the concentration overpotential increases with the increasing current density and electrode depths.
(4) For a low anode porosity case, the corrugated electrolyte shape did not enhance the cell performance and the maximum current density was observed at a high current density owing to the increasing concentration overpotential. Hence, it should be noted that anode porosity unfavourably affects enhancement by interface area enlargement if the anode porosity is extremely low.

Acknowledgements

This study is partially supported by the European Commission (project Dev-BIOSOFC, FP6-042436, MTKD-CT-2006-042436). This study is supported by the New Energy and Industrial Technology Development Organization (NEDO) under the Development of System and Elemental Technology on Solid Oxide Fuel Cell (SOFC) Project.

References

[1] N.M. Sammes, Y. Du, R. Bove, J. Power Sources 145 (2005) 428–434.
[2] J.-H. Kim, R.-H. Song, K.-S. Song, S.-H. Hyun, D.-R. Shin, H. Yokokawa, J. Power Sources 122 (2003) 138–143.
[3] Y. Lu, L. Schaefer, P. Li, J. Power Sources 140 (2005) 331–339.
[4] T. Suzuki, T. Yamaguchi, Y. Fujishiro, M. Awano, J. Power Sources 160 (2006) 73–77.
[5] J.J. Hwang, C.K. Chen, D.Y. Lai, J. Power Sources 140 (2005) 235–242.
[6] K. Sasaki, J.-P. Wurth, R. Gschwend, M. Gödickemeier, L.J. Gauckler, J. Electrochem. Soc. 143 (2) (1996) 530–543.
[7] L. Jia, Z. Lu, J. Miao, Z. Liu, G. Li, W. Su, J. Alloys Compd. 414 (2006) 152–157.
[8] J.R. Smith, A. Chen, D. Gostovic, D. Hickey, D. Kundinger, K.L. Duncan, R.T. DeHoff, K.S. Jones, E.D. Wachsman, J. Power Sources 180 (2009) 90–98.
[9] M.J. Jørgensen, P. Holtappels, C.C. Appel, J. Appl. Electrochem. 30 (2000) 411–418.
[10] D. Simwonis, F. Tietz, D. Stover, Solid State Ionics 132 (2000) 241–251.
[11] Y.L. Liu, S. Primdahl, M. Mogensen, Solid State Ionics 161 (2003) 1–10.
[12] A. Konno, H. Iwai, K. Inuyama, A. Kuroyanagi, M. Saito, H. Yoshida, K. Kodani, K. Yoshikata, J. Power Sources 196 (2011) 98–109.
[13] J.H. Nam, D.H. Jeon, Electrochim. Acta 51 (2006) 3446–3460.
[14] P. Costamagna, P. Costa, V. Antonucci, Electrochim. Acta 43 (1998) 375–394.
[15] E.A. Mason, A.P. Malinauskas, R.B. Evans III, J. Chem. Phys. 46 (8) (1967) 3199–3216.
[16] D. Arnost, P. Schneider, Chem. Eng. J. 51 (1995) 91–99.
[17] B. de Boer, Ph.D. Thesis, University of Twente, Netherlands (1998).
[18] Y. Suzue, N. Shikazono, N. Kasagi, J. Power Sources 184 (2008) 52–59.
[19] R. Radhakrishnan, A.V. Virkar, S.C. Singhal, J. Electrochem. Soc. 152 (1) (2005) 210–218.